Self-bending elastic waves and obstacle circumventing in wireless power transfer

S. Tol,[1] Y. Xia,[1] M. Ruzzene,[1,2] and A. Erturk[1,a)]

[1]*G. W. Woodruff School of Mechanical Engineering, Georgia Institute of Technology, Atlanta, Georgia 30332, USA*
[2]*D. Guggenheim School of Aerospace Engineering, Georgia Institute of Technology, Atlanta, Georgia 30332, USA*

We demonstrate self-bending of elastic waves along convex trajectories by means of geometric and phased arrays. Potential applications include ultrasonic imaging and manipulation, wave focusing, and wireless power transfer around obstacles. The basic concept is illustrated through a geometric array, which is designed to implement a phase delay profile among the array elements that leads to self-bending along a specified circular trajectory. Experimental validation is conducted for the lowest asymmetric Lamb wave mode in a thin plate over a range of frequencies to investigate the bandwidth of the approach. Experiments also illustrate the functionality of the array as a transmitter to deliver elastic wave energy to a receiver/harvester located behind a large obstacle for electrical power extraction. It is shown that the trajectory is not distorted by the presence of the obstacle and circumventing is achieved. A linear phased array counterpart of the geometric array is then constructed to illustrate the concept by imposing proper time delays to the array elements, which allows the generation of different trajectories using the same line source. This capability is demonstrated by tailoring the path diameter in the phased array setting, which offers the flexibility and versatility to induce a variety of convex trajectories for self-bending elastic waves. *Published by AIP Publishing.*
[http://dx.doi.org/10.1063/1.4981251]

Elastic/acoustic wave manipulation and guiding are of interest for several emerging fields and applications including structural health monitoring,[1] ultrasonic imaging,[2,3] cloaking,[4–7] contactless powering of wireless electronic components,[8–11] acoustic activation of drug delivery,[12,13] and acoustic manipulation.[14] Wireless elastic/acoustic power transfer[8–11] from a source to a remote receiver with minimum losses is critical to several of these applications. A plausible scenario is the powering of a sensor node that is otherwise beyond reach due to an obstacle between the transmitter and receiver. In other applications, it might be desired to minimize the intensity of propagating waves in certain structural regions. For instance, critical mechanical or electromechanical components that are sensitive and vulnerable to vibrations can benefit from curvilinear manipulation and circumventing of elastic waves through convex trajectories. Numerous other examples in the aforementioned research areas could exploit a convenient methodology for manipulating and guiding elastic waves along curved paths. Recent literature of elastic wave propagation reveals that most of the existing efforts on wave field guiding, manipulation, and cloaking explored metamaterials/metasurfaces and phononic crystals through complex structural configurations.[4–7,15–18]

Zhang *et al.*[19] recently demonstrated the generation of acoustic bottle beams through self-bending wave packets in two and three dimensional domains. The authors considered both a single and a collection of line arrays to guide the propagation of acoustic waves along trajectories described by Bézier curves. Their results demonstrate the robustness of propagation along the prescribed paths and the generation of a low pressure region within the region enclosed by such paths. The objective of our current work is to numerically and experimentally extend the approach in Ref. 19 to elastic waves propagating in plate-like structures along arbitrary convex trajectories. To this end, first a geometric array is constructed to follow a specified circular path. After experimental validation of numerical simulations, the geometric array is used for transferring elastic wave energy to an electrically loaded receiver behind a large obstacle. The phased array counterpart of the geometric array is also constructed and experimentally validated, along with additional case studies illustrating the tailoring of the curved circular path by changing its prescribed diameter.

The geometric array is designed by applying a ray tracing approach, which defines the distance of the source from each point on the desired trajectory. By applying simple geometric considerations, each source point is located at the intersection of two perpendicular lines to the tangents to two successive points on the assigned trajectory. The approach implements a proper phase relation among the element arrays that leads to constructive interference along the desired path. The same phase relations can be obtained on a linear array by imposing proper delays among the source elements, which is defined by back-propagating the excitation of each array element to its geometric counterpart. The spacing of the array elements is defined by the maximum number of sources that one chooses to employ and by the array aperture, which here is defined empirically to be sufficiently large to enclose the desired path. Figure 1 illustrates the

---

a)Author to whom correspondence should be addressed. Electronic mail: alper.erturk@me.gatech.edu.
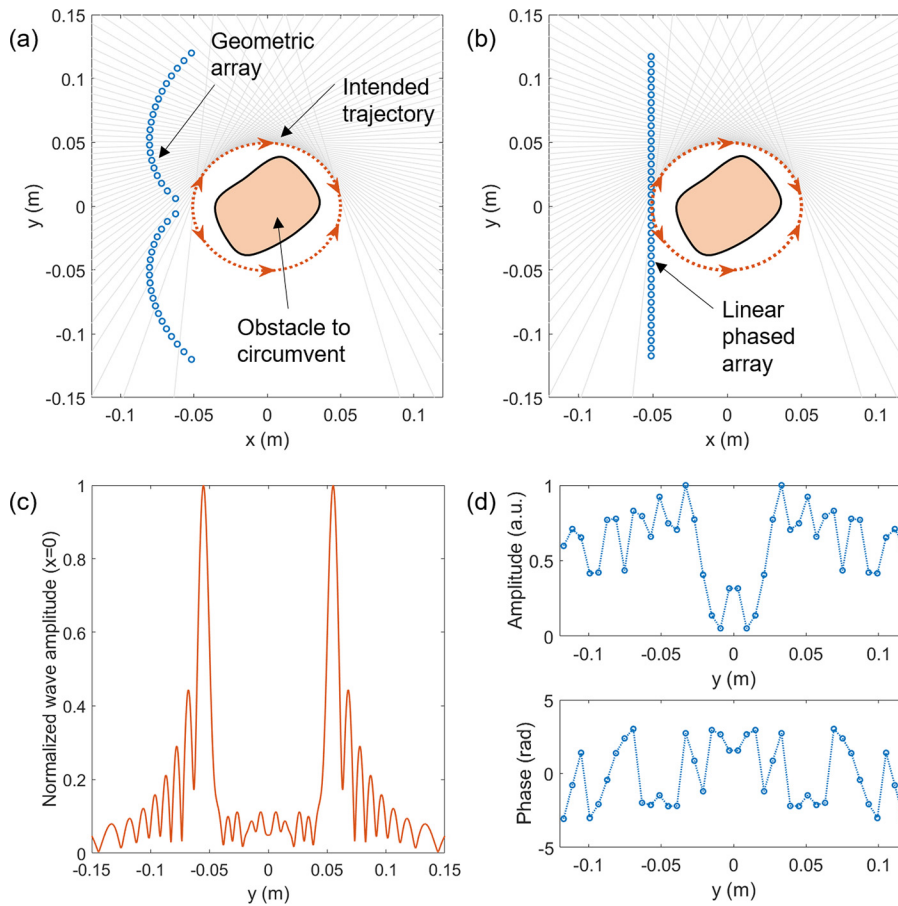
FIG. 1. (a) Geometric array and (b) linear phased array configurations to form the same circular trajectory (of 100 mm diameter) using a discrete array of 40 point sources; (c) the resulting normalized wave amplitude at the centerline ($x = 0$) of the circular path; and (d) amplitude and phase distributions for a phased array (b) made from a line array of 40 point sources to form a circular trajectory of 100 mm diameter.

formation of a circular path of a certain diameter (100 mm) by means of a geometric array (Fig. 1(a)) and by employing a linear phased array (Fig. 1(b)). The resulting wave intensity along the centerline of the circular path ($x = 0$) is shown in Fig. 1(c). The grey lines in Fig. 1(a) show the rays corresponding to the tangents to the trajectory, which are here plotted for the upper half (semi-circle) of the intended trajectory. This forms the upper half of the geometric array, which can be used to generate the lower half through symmetry. The amplitude and phase distributions of the line array sources, resulting from the geometric array designed based on a Green's function formalism[20,21] for back propagation, are shown in Fig. 1(d). The Green's function formalism is based on harmonic wave motion evolving in space according to the simplified form $\frac{1}{\sqrt{r}} e^{jkr}$, which includes cylindrical spreading losses, and where r denotes the distance from each point of the linear array to its geometrical counterpart, while k is the wavenumber of the considered wave mode, which here is the fundamental asymmetric Lamb wave mode (A_0). For practical purposes, the array is discretized in a finite number of sources, which are spaced based on wavelength considerations as discussed later in this paper. It is important to note that the circular trajectory will not fully close for the number of discrete sources shown in Figs. 1(a) and 1(b), which can readily be observed from the rays in Fig. 1(a) by drawing a tangent from the outermost source to the intended circular path.

The experimental setup employed for visualization of self-bending elastic waves and for demonstrating wireless power transfer by circumventing a large obstacle is shown in

Fig. 2. The geometric array (Fig. 2(b)) consists of 40 piezoelectric transducers (5 mm × 0.4 mm from STEMiNC Corp.) bonded to a 0.81-mm-thick rectangular aluminum plate that is large enough to distinguish the incident waves and boundary reflections. The phased array (Fig. 2(c)) setup consists of a linear array of the same type. The spacing between the transducers is of $d = 6$ mm, which is chosen based on the wavelengths corresponding to the frequency range relevant to A_0 mode propagation in the considered plate (30–100 kHz). In Fig. 2(d), the experimentally measured wave amplitude at the centerline of the circular path ($x = 0$) is plotted for different transducer spacing values (normalized by wavelength) and it is observed that the performance degrades when the transducer spacing exceeds the wavelength (cf. Fig. 1(c)). As the excitation frequency is increased from 30 kHz to 100 kHz (frequencies of interest in this work), the wavelength changes from 16.2 mm to 8.7 mm, and thus, the transducer spacing of $d = 6$ mm ensures that the dimensionless ratio d/λ changes from 0.4 to 0.7. Therefore, the aforementioned transducer spacing leads to a spatial wave intensity distribution that is similar to Fig. 1(c) and is effective at forming a clearly defined circular path.

The piezoelectric transducer array is excited by 4 cycles of sinusoidal burst at desired frequencies using a function generator (Agilent 33220A) and a high-voltage amplifier (Trek Model PZD350). The piezoelectric transducers in the geometric array are excited in phase with the same amplitude. A Polytec PSV-400 scanning laser Doppler vibrometer (LDV) is employed in order to measure the resulting wave field by recording the out-of-plane velocity of the plate
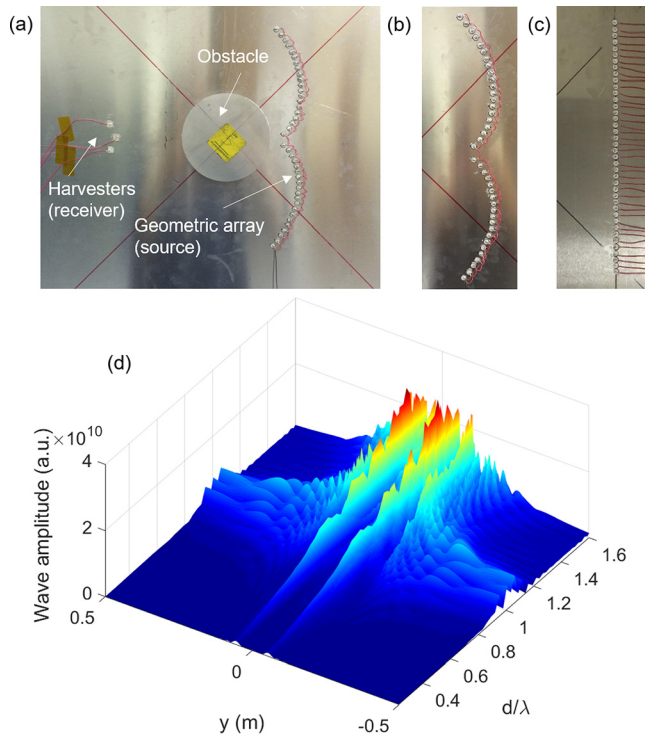
FIG. 2. (a) Experimental setup showing the specific configuration for wireless power transfer/harvesting by circumventing a cylindrical obstacle using a geometric array (the scanning LDV measures out-of-plane velocity field of the opposite face of the aluminum plate); close-up views of (b) geometric array and (c) linear phased array made from 40 piezoelectric patches; and (d) effect of transducer spacing on the performance of wave circumventing with a focus on the centerline of the circular trajectory, i.e., $x = 0$ (transducer spacing d is normalized by wavelength λ).
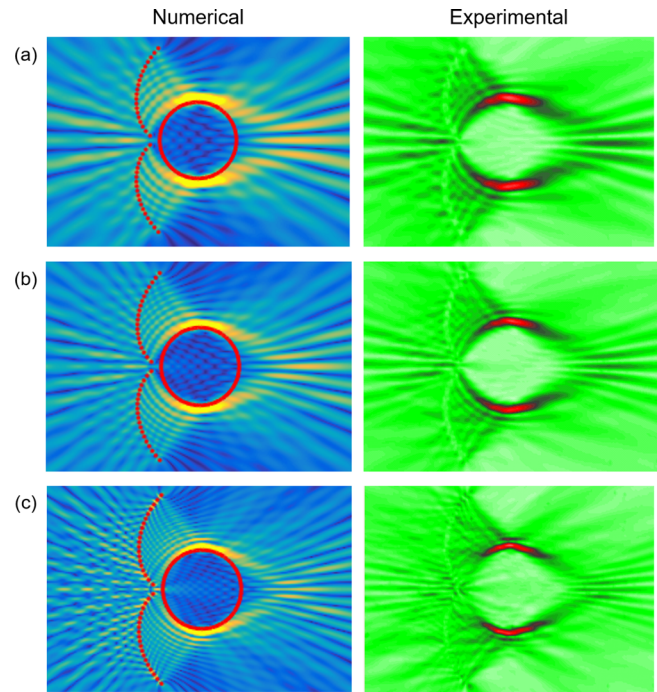

FIG. 3. Geometric array results showing the numerically simulated and experimentally measured RMS wave fields at different frequencies: (a) 30 kHz, (b) 50 kHz, and (c) 100 kHz.

(scanning is performed on the opposite flat face which is the back of the view in Fig. 2(a)) over a grid of points covering the geometric/phased array domain. With proper triggering of the LDV measurements, the wave field was reconstructed. The RMS (root-mean-square) values are obtained by integrating the measured response over time.

First, wave field simulations and experiments are conducted in the absence of the large obstacle shown in Fig. 2(a). Figure 3 shows the comparison of numerical simulations with experimental results for RMS wave field at frequencies selected over a broad range (30, 50, and 100 kHz). The geometric array in the experimental setup (Fig. 2(b)) is designed to form a circular trajectory with a diameter of 100 mm. The numerical results are obtained by computing the RMS of the wave field resulting from the superposition of point excitation at the locations of the array elements. Propagation from the source is described by the same Green's function formalism discussed above and based on wavenumber estimations for the plate and wave mode under consideration. The comparison of numerical and experimental RMS wave fields (out of plane velocity) shown in Fig. 3 reveals excellent agreement at all the considered frequencies.

In addition to validating the numerical simulations of the geometric array, the results in Fig. 3 unveil the *broadband* nature of the concept, i.e., roughly the same path can be achieved over a range of frequencies rather than at a fixed frequency (recall that this is strongly related to the transducer spacing in view of Fig. 2(d)—for 30, 50, and 100 kHz, d/λ = 0.4, 0.5, and 0.7). It can also be noted that the circular path

fails to close at the point diametrically opposite to the source location, which is consistent with the fact that a limited aperture for the array is considered based on practical considerations. Closing the circle would require the array to be constructed by considering tangents to the entire trajectory, which would lead to an array that physically fully encloses the prescribed path. This would defeat the primary purpose of the array and would lead to excessive practical complexity. Thus, the study explores the ability of the limited aperture array to still outline the desired path, which is confirmed by the results in Fig. 3.

Having validated the geometric array experimentally, next we explore the circumventing of a large cylindrical obstacle (shown in Fig. 2(a)) along with a case study of elastic power transfer to an energy-harvesting receiver behind this obstacle. The diameter of the obstacle is 95 mm, which is very close to the diameter of the intended path (100 mm). Furthermore, the thickness (i.e., out of plane height) of the obstacle is 12.7 mm, leading to an area of large impedance mismatch relative to the surrounding plate. An example RMS wave field is shown in Fig. 4(a) for 50 kHz excitation, remarkably confirming that the existence of this large obstacle does not distort the desired wave trajectory. The instantaneous wave field shown in Fig. 4(b) is useful in order to design the energy-harvesting receiver (which would represent the receiver near an inaccessible wireless sensor node in practice). A continuous harvester patch domain can be patterned by wave number transformation and out-of-phase portions can be wired accordingly as done by Carrara *et al.*[22] Instead, for simplicity, three maximum intensity in-phase portions (shown with a close-up in Fig. 4(c)) are exploited with three half-wavelength piezoelectric patches combined in parallel to form the receiver/harvester.
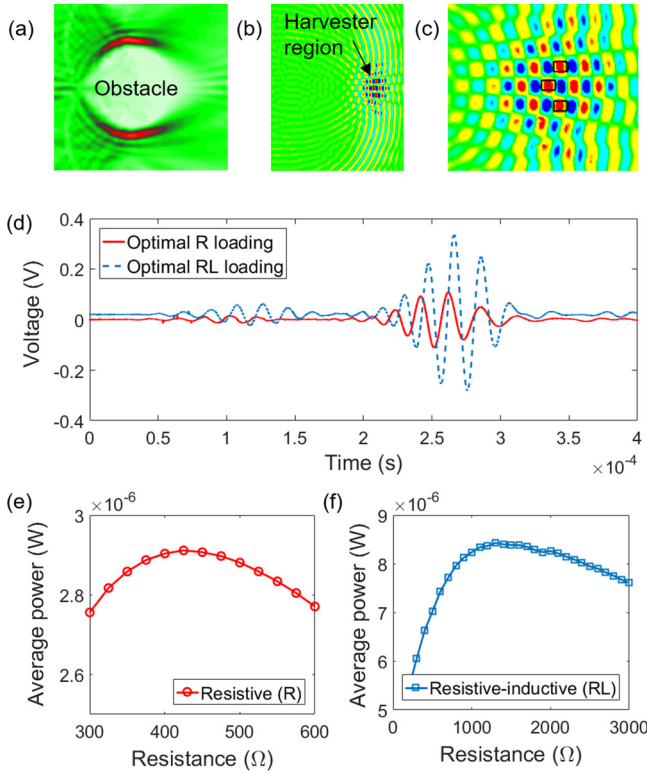
FIG. 4. Obstacle circumventing and energy harvesting results: (a) RMS wave field (for excitation at 50 kHz) confirming that the designed trajectory is not distorted by the presence of a large obstacle; (b) instantaneous wave field formed behind the obstacle and (c) close-up of the harvester region with a simple design (using three in-phase piezoelectric patches combined in parallel); (d) voltage waveforms of the receiver/harvester under optimal resistive and resistive-inductive loading (in response to a 4-cycle burst excitation at 50 kHz); (e) and (f) average power outputs under resistive and resistive-inductive loading cases vs. load resistance.
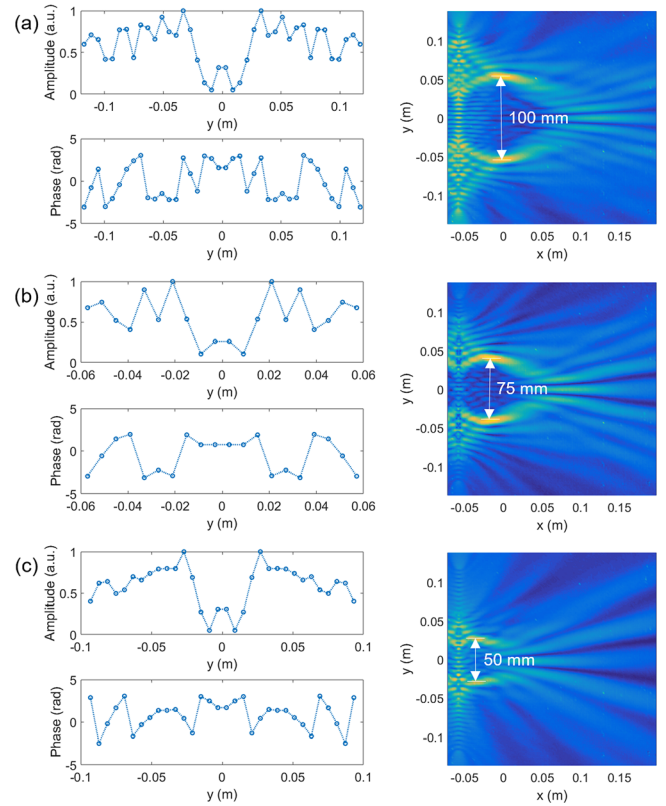

FIG. 5. Phased array results by superimposing the experimental wave fields generated by individual transducers with a proper amplitude and phase combination in order to form convex paths of different diameters: (a) 100 mm; (b) 75 mm; and (c) 50 mm.

Energy harvesting experiments are then performed through resistor sweep tests by shunting the bottom and top electrodes of the piezoelectric harvesters (three patches combined in parallel) to a range of electrical loads covering the optimal conditions. Both resistive (R) and resistive-inductive (RL) loading conditions are explored. The average power outputs of the harvesters were calculated from the voltage measurements across the resistor with an oscilloscope (Tektronix TDS3054). Voltage waveforms in response to incident wave packets are displayed in Fig. 4(d) for optimal resistive and resistive-inductive loading. The average power output across the electrical load was calculated from the RMS of the voltage waveforms, yielding Figs. 4(e) and 4(f) with changing load resistance, respectively, for resistive and resistive-inductive loading. While the maximum power is obtained for 425 Ω under purely resistive loading (which agrees with the optimal load resistance estimate by $1/\omega C_p$, where ω is the excitation frequency and C_p is the piezoelectric capacitance), three times larger maximum power output is obtained for resistive-inductive loading using 1300 Ω and 1 mH, as a result of complex conjugate impedance matching. It is worth mentioning that the intensity of the transferred micro-power can be enhanced dramatically by using a source array designed to give a proper Bézier curve[19] that fully closes at the receiver/harvester location. However, the current case study merely intends to demonstrate the possibility of

elastic wave power transfer behind a large obstacle, which can find applications for sensors and other wireless low-power components functioning in areas beyond reach due to other objects.

As a final case study, first we explore the formation of the same circular trajectory and then the tailoring of its diameter using the linear phased array shown in Fig. 2(c). Since simultaneous excitation of 40 transducers in experiments would require 20 source channels (for a path that is symmetric about y-axis in Fig. 1), as an alternative, the wave field created by each transducer is scanned and recorded (4-cycle burst excitation at 50 kHz) for superposition by adjusting the amplitude and relative phase. For instance, the amplitude and phase combination previously given by Fig. 1(d) yields the 100 mm diameter circular trajectory, as displayed in Fig. 5(a), which agrees well with the geometric array counterpart shown in Fig. 3(b). Next, the amplitude and phase distributions are obtained from the theory to create 75 and 50 mm diameter circular trajectories, which are obtained as shown in Figs. 5(b) and 5(c), respectively. Clearly, the linear phased array is dramatically more versatile to give various convex trajectories for proper amplitude and phase distributions.

In conclusion, this study has extended a recent acoustic framework[19] on self-bending beams to elastic structures. Specifically, we explored self-bending elastic waves guided along convex trajectories by means of geometric and linear phased arrays, which can find numerous applications related to wave manipulation and wireless power transfer by circumventing objects. The basic concept was illustrated for the lowest asymmetric Lamb wave mode using a geometric

array. Circumventing of a large obstacle was demonstrated along with a case study on wireless power transfer to a receiver/harvester behind the obstacle. A phased array was employed for tailoring the diameter of the designed trajectory by altering the amplitude and phase distribution of the array, offering significant versatility in generating various forms of self-bending elastic waves.

[1]Z. Su, L. Ye, and Y. Lu, J. Sound Vib. **295**(3), 753–780 (2006).
[2]H. Jia, M. Ke, R. Hao, Y. Ye, F. Liu, and Z. Liu, Appl. Phys. Lett. **97**(17), 173507 (2010).
[3]J. H. Oh, H. M. Seung, and Y. Y. Kim, Appl. Phys. Lett. **104**(7), 073503 (2014).
[4]S. Zhang, C. Xia, and N. Fang, Phys. Rev. Lett. **106**(2), 024301 (2011).
[5]N. Stenger, M. Wilhelm, and M. Wegener, Phys. Rev. Lett. **108**(1), 014301 (2012).
[6]S. A. Cummer and D. Schurig, New J. Phys. **9**(3), 45 (2007).
[7]D. Torrent and J. Sánchez-Dehesa, New J. Phys. **10**(6), 063015 (2008).
[8]M. G. Roes, J. L. Duarte, M. A. Hendrix, and E. A. Lomonova, IEEE Trans. Ind. Electron. **60**(1), 242–248 (2013).
[9]Y. Hu, X. Zhang, J. Yang, and Q. Jiang, IEEE Trans. Ultrason., Ferroelectr., Freq. Control **50**(7), 773–781 (2003).
[10]S. Shahab, M. Gray, and A. Erturk, J. Appl. Phys. **117**(10), 104903 (2015).
[11]H. Basaeri, D. B. Christensen, and S. Roundy, Smart Mater. Struct. **25**(12), 123001 (2016).
[12]A. Marin, M. Muniruzzaman, and N. Rapoport, J. Controlled Release **71**(3), 239–249 (2001).
[13]W. G. Pitt, G. A. Husseini, and B. J. Staples, Expert Opin. Drug Delivery **1**(1), 37–56 (2004).
[14]J. Shi, D. Ahmed, X. Mao, S.-C. S. Lin, A. Lawit, and T. J. Huang, Lab Chip **9**(20), 2890–2895 (2009).
[15]F. Casadei, T. Delpero, A. Bergamini, P. Ermanni, and M. Ruzzene, J. Appl. Phys. **112**(6), 064902 (2012).
[16]P. Celli and S. Gonella, J. Appl. Phys. **115**(10), 103502 (2014).
[17]C. Boutin, L. Schwan, and M. S. Dietz, J. Appl. Phys. **117**(6), 064902 (2015).
[18]H. Zhu and F. Semperlotti, Phys. Rev. Lett. **117**(3), 034302 (2016).
[19]P. Zhang, T. Li, J. Zhu, X. Zhu, S. Yang, Y. Wang, X. Yin, and X. Zhang, Nat. Commun. **5**, 4316 (2014).
[20]K. F. Graff, *Wave Motion in Elastic Solids* (Courier Corporation, New York, 2012).
[21]M. Carrara, M. Cacan, M. Leamy, M. Ruzzene, and A. Erturk, Appl. Phys. Lett. **100**(20), 204105 (2012).
[22]M. Carrara, J. Kulpe, S. Leadenham, M. Leamy, and A. Erturk, Appl. Phys. Lett. **106**(1), 013907 (2015).